Novel Hybrid Hypercrosslinked Polymer Assisted Highly Efficient Thermal Energy Storage

Changhui Liu (liuch915@cumt.edu.cn)
China University of Mining and Technology https://orcid.org/0000-0001-8265-7302
Jiahao Zhang
China University of Mining and Technology
Jian Liu
China University of Mining and Technology
Zengyi Tan
China University of Mining and Technology
Yuqi Cao
China University of Mining and Technology
Xia Li
China University of Mining and Technology
Zhonghao Rao
China University of Mining and Technology

Article

Keywords: phase change materials (PCMs), pourous material, Highly Efficient Thermal Energy Storage

Posted Date: January 22nd, 2021

DOI: https://doi.org/10.21203/rs.3.rs-152851/v1

Abstract

Though a range of methods has been dedicated to solving the leakage problems, a versatile method which can meet with the organic and inorganic phase change materials (PCMs) simultaneously still have not been seen. In this work, an organic/inorganic hybrid Silioxyl functional group containing polymer was synthesized and applied to encapsulated PCMs. Owing to the mild hypercrosslinking reaction conditions, which only requires the addition of catalytic amount of aqueous alkali solution, renders it to be tolerance towards both organic and inorganic PCMs. More importantly, the homogeneous state of the initiate state of the mixture allowed the ultimate PCMs encapsulation rate and the uniformly blending of the third nano-additives with the aim of thermal conductivity enhancement. Further study reveals that the presence of this hybrid polymers endows a unique self-cleaning property to the obtained phase change composite that it displays a good hydrophobicity towards water droplets. More importantly, this novel PCMs encapsulation protocol shows a good tolerance with varies of nanoparticles, including carbon based nanomaterial, metal oxide nanoparticles and inorganic oxide nanoparticles, which enables an utmost 600% thermal conductivity enhancement and 93.7% light-to-thermal conversion efficiency with a latent heat of 180 J/g without the observation of any leakage.

Introduction

Depletion of fossil energy has become a critical issue since the rapid development of industry and economy. The search for new energy resource alternatives and improve the energy conversion efficiency are the continuous endeavor of researchers.[1] Energy storage technology is considered as an effective way to solve the problem of mismatch between energy supply and application in terms of space and time. Thermal energy storage (TES) plays a vital role among various energy storage techniques.[2, 3, 4, 5] TES can be used to collect and store heat energy and release heat energy with the demand in the future. The forms TES can be classified into thermal chemistry energy storage, sensible heat energy storage, latent heat energy storage or a combination of some of them. Among the aforementioned forms, latent heat energy storage (LHTES),[6, 7] also termed as phase change energy storage, has been widely applied in practical due to the high energy storage density, small temperature fluctuation during the working stage.[8, 9]

Phase change materials (PCMs) are functional materials that can absorb or release thermal energy in the form of latent heat within a certain temperature range.[10, 11, 12] PCMs can be generally divided into four forms in terms of phase change states, namely, solid-solid, solid-liquid, liquid-gas and solid-gas.[13, 14, 15] Solid-gas and liquid-gas PCMs benefit from high phase change energy storage density, however, the large volume change of material during phase transition makes it is difficult to be used in practical.[16] Solid-solid PCMs bearing the advantages of small volume change and low degree of supercooling,[17] but either suffer from low thermal energy density or limited temperature scope.[18, 19, 20] Solid-liquid type phase change is the most common and widest utilization form because of its negligible volume change during the phase transition process and high energy storage density. However, people must face the problem of

liquid leakage during the phase change process in solid-liquid phase change type associated with the poor thermal conductivity which would thus lead to its limited application scope.[21] Therefore, a shape-stabilized phase change material (SSPCM) which generally constituted by a working material and a supporting material has emerged as an important protocol for the use of solid-liquid phase change material.[22, 23, 24] The main methods for the preparation of shape stabilized PCMs are as follows: (1) Encapsulated PCMs into micro/nano capsules;[25, 26] Such as, Kawaguchi et al.[27] firstly reported a novel PCMs applications for high temperature(400-500˚C) by using Zn-30wt%Al alloy as wall material to encapsulate PCMs. The wall material of MEPCMs was composed of ZnO with a thickness of 500 nm and Al-oxide with a thickness of 300 nm. The phase transition temperature is 437-512 ˚C and the latent heat is 117 J/g. (2) Blending the solid-liquid PCMs with a porous materials in a simple physical fusion way;[28, 29, 30] representatively, Liu et al.[4]reported a new Lewis acid-catalyzed *in-situ* phase change PCMs shape stabilization strategy to prepare cross-linked polystyrene (HCPS) encapsulated PCMs to achieve efficient thermal energy storage objectives. Simultaneous crosslinking and encapsulation processes enable the strong $FeCl_3$ to catalyze crosslinking reactions, resulting in a high efficiency encapsulation rate. Conversion of $FeCl_3$ into Fe_3O_4 through simple alkali treatment can improve the thermal conductivity of PCMs, which can be increased by 17% ~ 55% compared with pure paraffin. (3) Electrostatic spinning technology;[31, 32, 33] For example, The polyethylene glycol composite PCMs (PCMs) containing boron hydroxylated Ni-Tride (BN-OH), cellulose nanofibers (CNF) and chitosan (CS) were prepared by *in-situ* ionic crosslinking with polyelectrolyte composite spinning by Fang et al.[34]. The results showed that the thermal conductivity of PCMs containing 47.5 wt% BN-OH reached 4.005 W/mK, which was 22.56 times that of pure PEG. (4) Grafting PCMs into the skeleton of the polymer through a covalent bond association way.[35, 36] For instance, Du et al.[26] successfully prepared a novel composite PCMs based on polyethylene glycol (PEG), nanofibrotic cellulose (NFC) and graphene by impregnating PEG into a PEG-grafted NFC/graphene-hybridized aerogel (GA/ NFC-G-PEG),Through grafting PEG to NFC, the affinity of PEG to NFC/graphene hybrid aerogel was improved, the PEG loading capacity of CNF-G-PEG/graphene aerogel was significantly improved, and PEG leakage was prevented. Though so many existed methods dedicated to developing a way for the solution of liquid leakage and poor thermal conductive performance,[37] the room for further improvement still existed.[38, 39] Such as sophisticated preparation process, which generally requires the addition of extra chemicals or harsh reaction conditions. On the other hand, the participation of supporting materials will inevitably reduce the energy storage density as the it has no contribution on the latent enthalpy.[40, 41] Therefore, an efficient way which could enhance the thermal conductivity on the premise of keeping the thermal energy storage density is also in highly demand.[42, 43, 44] To achieve this goal, previously we used polystyrene and PPh_3 as precursors to encapsulate PCMs, in which an $FeCl_3$ catalyzed and 1,2-dimethylmethane aided hypercrosslinked is the key factor that effect the encapsulation rate and thus impact the final thermal properties of obtained PCMs composite. In this process, we found that the moisture has a great influence on the success of encapsulation reaction since $FeCl_3$ is to sensitive towards the moisture which thus leads to the failure of Friedel-Crafts reaction behind.[45] To overcome this inherent drawback, we envisioned that whether we

could graft a functional group that easy to be crosslinked on the skeleton of monomer, which thus deemed to participate in the hypercrosslinked reaction without the need of harsh reaction condition. In this work, for the first time, we synthesized a -Si-O- containing polymer, which could be crosslinked under a mild condition and formed a porous structure after integrating with a nanomaterial. More importantly, our study revealed that the presence of -Si-O- group could serve as a micro water reservoir which was able to prevent the loss of bounded water from inorganic PCMs, which thus ensured a good encapsulation efficiency and recyclability. Blending the other material with a high thermal conductivity is a common way to enhance the thermal conductivity of PCMs composites.[46, 47] However, it also suffers the risk of phase separation during the phase transition state, thus causes the invalidation of the energy storage function. Wrapping PCMs with a polymer is a good solution towards the problem, while it should also face the solubility and compatibility between PCMs and that of polymers.[48] In this work, we adapted a homogeneous-to-heterogeneous protocol, mixing PCMs with soluble linear polymer prior to PCMs holding process and then initiates the hypercross-linking reaction *via* a simple alkali treatment. This method was able to ensure the utmost uniform and even mixing of PCMs and nanoparticle and avoid the phase separation in the downstream real application case. It is worth noting that our protocol is allowed the incoropation with several different nanoparticles, such as, graphene, SiC, carbon black, SiO_2, etc. Due to the synergistic contribution from polymer and nanoparticles, the highest thermal conductivity can achieve to 600% with a light-to-thermal conversion up to 93.7% without observation of any liquid leakage with respect to both organic and inorganic PCMs.

Results And Discussion

Preparation and characterization of the resulting materials

Our study commenced from the synthesis of the hybrid polymer. The reaction was carried out in a nitrogen atmosphere by employing AIBN as a radical initiator. The proportion of styrene (organic part) and silica containing styrene (inorganic part) was facilely tuned by the amount of two different starting materials. As it is shown in **Fig. 1** and **Fig.S1**, integration in ^{1}H NMR shows a good agreement with the proportion of the two parts. After obtaining the hybrid polymer, the preparation of the PCMs composite was initiated. As a proof-of-concept, the preparing technique was designed based on a homogeneous-to-heterogeneous protocol with the aim at solving the poor encapsulation efficiency along with the compatibility problem between PCMs and thermal conductivity enhancement nanoparticle. In order to realize the optimized preparation conditions in terms of encapsulation efficiency and energy storage density, some parameters were subjected to examination (Table S2 and S3). In order to facilitate the screen process, we firstly fixed the mass of paraffin, carbon black and the hybrid polymer and studied the effect the proportion of these two different monomers. As it is displayed in Table 1, the leakage of PCMs was up to 8.7% in the absence of a hybrid polymer. It also reveals that carbon black was also capable for the holding of PCMs due to its porous structure inside, however, the performance of sole carbon black is far to satisfactory. The leakage rate drastically reduced to 4.28% owing to the contribution of the hybrid polymer, it provides both binding effect and more fertile pore to carbon black, which might act as a

holding material in the process. Our protocol exerts the occurrence of hypercrosslinking reaction under an alkali condition on the premise of the presence of silica containing monomer, which could couple with each other via a cascade intermolecular electrophilic substitution and elimination and thus delivers the hypercrosslinking reaction. Under this consideration, we are interested in the concentration of monomer B as it directly determines the hypercrosslinking rate of the hybrid polymer. As it is shown in **Fig. 2g**, the leakage rate really displays a decline trend with the concentration rising of monomer B, and the leakage rate could low to 0.3% after blending a hybrid polymer with a 1:1 of monomer A and monomer B. Owing to the relatively high cost of the silica containing monomer and the acceptable 0.3% leakage rate, the continue increase on the proportion of monomer B was not carried out. After knowing the trend on the chemical composition of hybrid polymer, we started to investigate the effect of total mass of polymer. As it is predicted, the leakage rate gradually increased with the weight decrease of the hybrid polymer. This result further demonstrates function of the hybrid polymer that it was able to encapsulate paraffin during the phase transition process (**Fig. 2h**). Additionally, compared with hybrid polymer, carbon black displays a slight influence on the carrying performance of the PCMs composite since the leakage efficiency kept almost unchanged in the case of 0.4 g hybrid polymer associated with 4 g carbon black (entry 11) by a comparison with that case of 0.5 g hybrid polymer and 5 g carbon black (entry 7) (**Fig. 2i**). Further decreasing the total amount of supporting materials unexpectedly led to the rising of leakage rate which demonstrated the synergistic effect between the polymer and carbon black (entry 12). Moreover, a control experiment was carried out to illustrate the importance of the hypercrosslinking reaction in the process. As shown in entry 13, the PCMs composite gives a comparable encapsulation performance with the sole carbon black supported PCMs composite without the addition of a base solution, which clearly demonstrated the occurrence of the hypercrosslinking reaction and success of the encapsulation of PCMs after an alkali treatment.

Table 1. Different reaction parameters.

entry	Sample name[a]	Molar ratio of polymer monomers	Mass of polymer (g)	Mass of carbon black (g)	Leakage rate (%)
1	CB-PCMs[a]	\	\	5	8.7
2	HP/CB-OPCMs (9:1)[b]	9:1	0.5	5	4.28
3	HP/CB-OPCMs (8:2)[c]	8:2	0.5	5	2.36
4	HP/CB-OPCMs (7:3)[d]	7:3	0.5	5	1.28
5	HP/CB-OPCMs (6:4)[e]	6:4	0.5	5	0.45
6	HP/CB-OPCMs (5:5)[f]	5:5	0.5	5	0.3
7	HP/CB-OPCMs (5:5)[f]	5:5	0.4	5	1.68
8	HP/CB-OPCMs (5:5)[f]	5:5	0.3	5	2.63
9	HP/CB-OPCMs (5:5)[f]	5:5	0.2	5	4.75
10	HP/CB-OPCMs (5:5)[f]	5:5	0.1	5	5.88
11	HP/CB-OPCMs (5:5)[f]	5:5	0.4	4	1.32
12	HP/CB-OPCMs (5:5)[f]	5:5	0.3	3	3.54
13	HP/CB-OPCMs (5:5)[g]	5:5	0.5	5	7.9

[a] Unless otherwise stated, the mass of all added carbon black is 5g, and the melting phase transition temperature of paraffin is 60 ^{o}C. [b] For the preparation of polymer, monomer **A** is styrene (PS), monomer **B** is trimethoxy (4-vinylphenyl) silane, styrene (5.0 g), trimethoxy (4-vinylphenyl) silane (1.2 g), AIBN (15.8 mg) and trichloromethane (10 ml). [c] styrene (0.75 g), trimethoxy (4-vinylphenyl) silane (0.404 g), AIBN (15.8 mg). [d] styrene (2.0 g), trimethoxy (4-

vinylphenyl) silane (0.922 g), AIBN (6.3 mg). [e] styrene (1.0 g), trimethoxy (4-vinylphenyl) silane (1.43 g), AIBN (3.15 mg). [f] Styrene (1.0 g), trimethoxy (4-vinylphenyl) silane (2.15 g), AIBN (6.3 mg), [g] phase change material composites without alkali treatment.

After determining the optimized preparation parameters and the preparation procedure, structural analysis on the obtained PCMs composite was carried out. As it is displayed in **Fig. 2a** and **Fig. S4**, SEM images of the PCMs composites reveal that PCMs were either encapsulated on the pore and surface of the supporting materials without the observation of liquid state paraffin. This result also directly proves the success of our solid-liquid PCMs shape stabilization protocol as the SEM taking temperature is much higher than its phase change transition temperature. Interestingly, a phenomenon could be observed that a distributed uniformly nano-scaled wire was found in this hybrid polymer encapsulated PCMs composite which can be attributed to the participation of the hypercrosslinked hybrid polymer. Further study revealed that the concentration of the nano-wire unambiguously increased with the dose rising of the hybrid polymer. From this result, we can roughly conclude that the hypercrosslinked polymer not only provide a porous structure for the holding of paraffin wax, but also acts as a well-distributed wire to bind the carbon black/paraffin composite to prevent the leakage of paraffin under a condition that higher than that of phase change temperature. Besides the micro structure of the PCMs composite, some chemical composition analysis was performed. As shown in **Fig. 2e**, FT-IR spectra indicates that the main characteristics of the composite material mainly derived from the contribution of paraffin in which the peaks at 2920cm^{-1} and 2850cm^{-1} are asymmetric stretching vibration of -CH_2 and symmetric stretching vibration of -CH_2, respectively. The swaying vibration of -CH_2 group was responsible for the peaks at 1465 cm^{-1} and 720 cm^{-1}, and the peak at 1377cm^{-1} is attributed to the deformation vibration of -CH_3. On the other hand, the peak strength gradually decreased with the portion rising of carbon black which further demonstrates the fact that carbon black is capable to absorb light whose wavelength lies in the infrared range. XRD were also subjected to analysis to understand the chemical properties of the PCMs composite. From the XRD patterns (**Fig. 2d**), we can clearly find that carbon black and polymer display their characteristic peaks at 2θ = 24.8°, 2θ =14.92° respectively in a testing range from 10° to 70°. The main signals of XRD patterns with respect to the PCMs composites with varies dose of carbon black and paraffin is in line with the characteristic peaks of pure paraffin and carbon black, which clearly excludes possibility of chemical interaction between each component and also proves the tolerance of this protocol towards the hybrid polymer and paraffin. Moreover, based on the TGA patterns of composite material shown in **Fig. 2f**, the paraffin keeps stable until a heating temperature higher than 200 °C and begins to lose weight after 250 °C due to the fracture of the paraffin molecule. The main weight loss of polymer appeared in a temperature range from 300 °C to 450 °C partially owing to the decomposition of the benzene ring. It should be noted that the decomposition temperature of the PCMs composite is much higher than that of pure paraffin, it can be probably ascribed to the shielding effect given by the hybrid polymer and carbon black. It also presents a fact that this kind of polymer and carbon black supporting material displays a certain positive effect on the thermal stability of the PCMs composition. Additionally, weight loss of the PCMs composite, which mainly comprises the thermal decomposition from paraffin and polymer inside without the observation of the other weight loss peaks, further demonstrates that

paraffin and polymer should be kept intact during this alkali promoted hypercrosslinking reaction process.

Moreover, to understand impact of paraffin on the hypercrosslinking reaction, we performed some control experiments. It is well known that the specific surface area of the material heavily determines the adsorption capacity of the supporting materials. In this regard, we prepared two types holding materials and sent to N_2 BET analysis, namely, hybrid polymer integrated carbon black composites in the absence of paraffin, hybrid polymer integrated carbon black with paraffin and then washed out paraffin before BET analysis. As it is displayed in **Fig 2b** and **2c**, the BET value of both samples shows an enhancement on BET value compared with that of pristine carbon black, and the later one even exhibited a higher specific area than that of samples without the addition of paraffin (Table 2). This results clearly exclude the negative impact of paraffin on the alkali mediated hypercrosslinking reaction, and more importantly, the presence of paraffin might benefit for the formation of the porous structure due to the enhanced dispersing effect which given by the organic component in the reaction system.

Table 2 Surface area and total pore characteristics of the as-synthesized samples.

Sample	BET surface area/(m^2/g)	Pore volume /(cm^3/g)	Average pore diameter /(nm)
CB+HP	131.54	0.59	17.93
CB	121.83	0.85	27.91
CB+HP+PW(washed pw)	151.14	0.39	10.25

Thermal physical performance of the resulting materials.

With the optimized preparation method and the corresponding PCMs composite, study on the thermo-physical properties was initiated. At the first, thermal conductivity of the obtained PCMs composite was analyzed because it is one of the most important parameters to evaluate the performance of shape-stabilized PCMs as it associates with the energy storage and release response time and thus determines the application efficiency. Whereas, low thermal conductivity problem was widely found in PCMs and thus limited its practical application. In this work, different thermal conductivity of PCMs composites were tested by a transient plane source method in which the measuring temperature ranges from 303 K to 333 K and tested every 5 K, depicted in **Fig. 2j** The thermal conductivity of HP/CB-OPCMs (5:5) can achieve to 0.5-0.6 W (m^{-1} K^{-1}), which is approximately 250% higher than that of pure paraffin (0.22-0.24 W (m^{-1} K^{-1})). Moreover, thermal conductivity of PCMs composite shows a slight variation under a testing temperature lower than the phase change temperature, but it fluctuates greatly with the temperature under a testing temperature higher than the phase transition temperature. The liquid state of the paraffin inside the porous structure might responsible for this phenomenon due to its inherent instability property

in terms of thermal conductivity. On the other hand, the existence of hybrid polymer displays a slight impact on the final thermal conductivity of PCMs composite, which means the presence of polymer would not ruin the continuous network mainly constructed by the carbon black and paraffin composition. This result further demonstrates the feasibility of our PCMs shape-stabilization protocol that the participation of hybrid polymer was able to prohibit the leakage of PCMs during the phase transition process without effect on the formation of the thermal transportation means provided by the high thermal conductivity nano-additives.

Energy storage density of the obtained PCMs composites, represents in the form of latent heat enthalpy, was measured in a way of DSC. As it is shown in **Fig. 2k**, the energy storage characteristics of PCMs with respect to both phase change temperature and enthalpy were measured by DSC for all samples. It can be seen from Table 3 and **Fig. S5** that both pristine paraffin and shape-stabilized materials show two peaks in both melting and solidification process, which were respectively attributed to solid-solid phase transition and solid-liquid phase transition of paraffin in the phase transition process. Through the synergic action of carbon black and polymer, it can be seen that HP/CB-OPCMs (5:5) has a slight temperature variation during the phase transition process, and the peak temperature of the melting process and solidifying process shift from 55.62°C and 50.82°C to 56.36°C and 50.32°C respectively. The reason responsible for this low temperature change can be ascribed to the good affinity between hybrid polymer and paraffin, which further affects the vicinal organic paraffin molecules in this three-dimensional network structure, thus delaying the phase transition process of the paraffin. More importantly, as it is shown in **Fig. 2l** and Table 3, this hybrid polymer carried PCMs shows a promising cyclability that it was able to keep almost unchanged with respect to both phase transition temperature and latent heat after a 500 times melting and solidification process. Moreover, leakage performance of the PCMs composite was further determined by using a digital camera along with an infrared camera. As shown in **Fig. S3**, the leakage-proof performance is quite in line with the leakage rate calculated with an accurate balance. Considering the excellent encapsulation efficiency, promising latent heat storage and the charging-discharging reliability, this hybrid polymer supported PCMs composite possessing a great potential to be used as an ideal thermal energy storage medium, especially in the practical scenarios.

Table 3 Data for the DSC curves for the HP/CB-OPCMs samples.

Sample	Melting process			Process of freezing		
	Onset (ºC)	Peak (ºC)	ΔH_m (J/g)	Onset (ºC)	Peak (ºC)	ΔH_m (J/g)
PW	49.55	55.62	188.62	53.62	50.82	185.36
CB-OPCMs	49.96	55.98	87.48	57.52	49.90	84.95
HP/CB-OPCMs (9□1)	49.24	57.39	82.40	53.51	49.62	79.79
HP/CB-OPCMs (8□2)	49.63	55.35	82.46	53.69	50.82	80.11
HP/CB-OPCMs (7□3)	49.53	56.66	87.29	53.62	49.98	85.19
HP/CB-OPCMs (6□4)	48.74	56.81	88.34	53.44	50.28	87.33
HP/CB-OPCMs (5□5)	49.06	56.36	82.62	53.55	50.32	82.30
HP/CB-OPCMs (5□5)[a]	49.83	56.45	80.46	53.28	49.04	75.292
HP/CB-OPCMs (5□5)[b]	49.92	55.65	80.93	53.31	49.61	76.65
HP/CB-OPCMs (5□5)[c]	50.08	55.68	80.17	53.39	49.70	76.73
HP/CB-OPCMs (5□5)d	50.09	55.52	79.44	53.42	49.88	75.54
HP/CB-OPCMs (5□5)f	50.26	55.71	79.02	53.33	49.82	74.74

[a] DSC data after cycling 100 times. [b] DSC data after cycling 200 times. [c] DSC data after cycling 300 times. [d] DSC data after cycling 400 times. [f] DSC data after cycling 500 times.

Real application of the resulting materials

To test the practical feasibility of this hybrid polymer encapsulated PCMs composite, some application study was carried out. On the first hand, thermal energy storage and release performance of the obtained PCMs composite was studied using a home-made setup. As it is shown in **Fig. 3a** and **Fig. S9a**, the platform was mainly composed by a heat storage and release unit, a data analysis unit and temperature regulation unit which was controlled by a water bath. The detail size of each unit was shown in **Fig. 3b**, to verify the position effect on the thermal energy storage efficiency, two different testing spots were set on different height. As can be seen from **Fig. 3c** and **3d**, neither T1 nor T2 could forward a prompter response during the heat energy charging process for the hybrid polymer encapsulated PCMs composite than that of pristine paraffin thanks to the superior thermal conductivity. However, when the temperature approaches to the melting temperature, the slope of temperature change of pristine paraffin overwhelms that of shape-stabilized PCMs composite probably owing to the thermal resistance deriving from the inherent swelling property of carbon-based materials supported PCMs composite. Similar phenomenon was observed in the thermal energy releasing process as the temperature responses rapidly for the hybrid polymer encapsulated PCMs composite (**Fig. 3e** and **3f**). Besides the thermal energy storage and release property regarding the obtained PCMs composite, light-to-thermal conversion performance of this shape-stabilized PCMs composite was also subject to study. As a kind of clean and sustainable energy, solar energy has been applied in many fields. However, the instability of solar energy in time heavily limits its application scope. However, solar energy collection technology or the storage of solar energy in materials and the conversion of solar energy into another kind of energy can solve this shortcoming well. **Fig. 3g** is the photothermal conversion curve of HP/CB-OPCMs(5:5) and pure paraffin using a photothermal conversion device. As you can see in **Fig. 3h** and **3j**, the initial temperature of the two materials are the same (30°C), under a 110 mW/cm^{-2} sunlight simulation condition, the temperature of the sample and pure paraffin increased with illumination time, but the temperature rise rate of the PCMs composite is much prompter than that of pure paraffin owing to the superior light response ability derived from carbon black inside. As it can be seen in **Fig. 3i**, after an exposure at a simulation sunlight device for 300s, the maximum temperatures reached by PCMs and pure paraffin were 63°C and 47°C respectively, increased by 33°C and 17°C respectively. More importantly, the phase transition phenomenon can be obviously observed in the case of PCMs composite, however, the pristine paraffin can not reach a phase transition temperature under the same irradiation condition, which further demonstrated the light-to-thermal conversion advantages thanks to the presence of carbon black. The sharp temperature dropping curves when turned off the light also proves the superior thermal conductivity of the PCMs composite, but the difference was shown to be smaller than that of light harvesting process which further proved the fact that main reason responsible for this result is the contribution of carbon black on good light-to-thermal conversion characteristic. Based on the temperature change curves of the hybrid polymer encapsulated PCMs composition and the latent heat of the PCMs composite, the light-to-thermal conversion efficiency was calculated to be 93.7%. It should be noted that light-to-thermal conversion of this PCMs composite is quite promising considering its relatively low thermal conductivity (**Fig. 3k**). Generally speaking, a higher thermal conductivity will benefit to the light harvesting due to the corresponding rapider energy transportation, but it will also lead to a harder conservation to some degree. From the viewpoint of the relatively low thermal conductivity and excellent light-to-thermal conversion efficiency, this PCMs

encapsulation protocol really protocol really provides a practical method for the fabrication of solar utilization materials.

Additionally, the hypercrosslinked polymers not only help encapsulate the paraffin but also good for the hydrophobicity increase of the surface of the PCMs composite. Superhydrophobicity of materials has drawn ample attention owing to its unique advantages, such as self-cleaning, water-proof, anti-corrosion and so on. Surface modification or spraying are commonly used approaches for the set of hydrophobicity, but they must face the inherent shortcomings due to the susceptibility brought from physical or chemical fragility of the micro structure. In this regard, we used a homogeneous-to-heterogeneous strategy, by which an even blending among the hypercrosslinked polymers, carbon black and paraffin can be unambiguously expected, thus could ensure a stable and long-term hydrophobicity. As shown in **Fig. 4a** and **Fig. S9b**, a water contact angle analysis platform was set and comprised by a testing unit, a high-speed camera and a data analyzer unit. PCMs composite without the addition of the hypercrosslinked polymer displays a water contact angle to be 99º might be accounted by the intrinsic hydrophobicity of paraffin and the rough surface due to the carbon black. As a result of addition of hybrid polymer, the water contact angle to can be significantly increased 120º, and it can be further increased to 137º when changed the polymer to a 5:5 monomer ratio (**Fig. 4c, 4d** and **4h**). Based on this interesting result, we proposed a plausible mechanism that the silica content should be help for the enhancement of hydrophilicity of the obtained PCMs composite as silica-oxygen bond is a polar functional group which will form a weak vander walls force with water molecule and therefore produced a good compatibility with that of water. However, the silica content also determines the hypercrosslinking rate of the hybrid polymer, it is predictable that the hypercrosslinking skeleton features a hydrophobicity as its main framework is constituted by organic alkane chain. Owing to the bulker property of organic component compared with silica group, the main contribution of this hybrid polymer should be hydrophobicity, and that's why the addition of the hybrid polymer was able to make a hydrophobicity increment (**Fig. 4b**). On the other hand, the presence of silica will allow the hydrophilicity increase, in the meantime, it also leads to the enhancement of hypercrosslinking and thus affords the rising of hydrophobicity. Out of this consideration, the final PCMs composite displays a phenomenon of hydrophobicity increase compared with that of PCMs without the addition of hypercrosslinked polymer.

Characterization of inorganic materials

Comparing with organic PCMs, inorganic PCMs bearing some unique advantages, such as high latent heat capacity, good thermal conductivity, promising fire-proof performance, non-toxic and so on.[54, 55, 56] However, some specific shortcomings of inorganic PCMs, for example, large supercooling characteristic, phase separation during the phase transition process, still heavily hamper the way of its widely application. Shape-stabilization strategy provides a feasible venue for the practical utilization of inorganic PCMs.[57, 58, 59] For example, Yang et al.[60] obtained hybrid properties by combining sol-gel method with interfacial polymerization, taking calcium hexahydrate (CCH) as the representative polychlorinated biphenyl (PCMs) of salt hydrate as the core material, and using organic alkoxysilane as the medium of hydrophilic core material and hydrophobic shell material. The Fourier transform infrared

spectra and SEM images confirmed that siloxane and polyurea shells successfully encapsulated the CCH core layer. Fu et al.[61] developed a novel phase change temperature-regulated composite phase change material using sodium acetate trihydrate and urea non-eutectic mixture as phase change material and gas-phase silicon dioxide (SiO2) as supporting material and temperature regulator. The results show that when the SiO2 mass fraction is 30%, the composite PCMs has the appropriate melting temperature (35.75 ºC), high latent heat (151.6 J/g) and low undercooling (1.14 ºC). Meanwhile, the composite PCMs has good morphological stability, excellent thermal reliability and good thermal conductivity. Xiao et al.[62] prepared a novel polycrystalline phase change hydrogel (LTPCH) composed of NaAc center point 3H(2)O, acrylamide-acrylic acid sodium copolymer and CuS by melt impregnation method. The morphology, thermophysical property, photothermal conversion property and cycle life of the prepared LTPCHs were investigated. The fluid leakage test showed that LTPCH containing 3H(2)O at the center of 87 wt% NaAc maintained the solid-gel structure during the phase transition, and there was no liquid leakage. Though some endeavors have been dedicated to the practical use of inorganic PCMs, a simpler and accessible way is also highly in demand. In this work, a new hybrid polymer aided homogeneous-to-heterogeneous protocol was developed, the outstanding superiority of this protocol is mainly ascribed to its compatibility towards water as the hypercrosslinking reaction was initiated by just adding catalytic amount of aqueous sodium hydroxide solution, which thus allows the preparation of both inorganic and organic PCMs composites. We chose sodium acetate trihydrate (SAT) as an inorganic phase change material and subject to the preparation of the PCMs composite using the above-mentioned homogeneous-to-heterogeneous protocol (the detail preparation process can be seen in supporting materials). To verify the availability of our protocol in the synthesis of inorganic PCMs, some preliminary experiments were conducted. The encapsulation efficiency of the composite was studied. As it is shown in **Fig. S8**, water loss phenomenon of SAT/carbon black composite was clearly observed as the surface of the composite gradually changed to white due to the precipitation of sodium acetate under a heating condition (the video of water loss process was recorded and shown in supporting materials). Interestingly, the water loss phenomenon alleviates significantly after adding the hybrid polymers during the preparation process. More importantly, samples with different hybrid polymer display different performance regarding water loss, and the larger proportion of silica containing monomer could deliver a better performance on the restriction of water loss. Based on this interesting phenomenon, we tried to explain the result in molecule scale. The results might derive from two aspects. Firstly, the presence of silica group on the skeleton of polystyrene could lead to the hypercrosslinking reaction due to the cascade substitution and elimination reaction between silicoxyl groups, the proportion increase of silicoxyl groups would inevitably make the increase of the hypercrosslinking rate between the pristine linear polymer which thus results in the formation of a porous structure bearing a larger specific surface area. On the other hand, the presence of silicoxyl group on the hypercrosslinked polymer could act as a micro water conserver, similar with a water sponge, which could thus restrain the bound water from loss owing to it intrinsic hydrophilicity (**Fig. 5f**). In order to support our hypothesis, some experiments were carried out. As it is seen in **Fig. S10**, the flow ability of the polymer was obviously hindered after the addition of aqueous sodium hydroxide due to the confinement of water in the hypercrosslinked polymer. Moreover, the leakage rate of this inorganic phase change material composite can be significantly reduced from 14.5% to 0.1% after blending SAT

and carbon black with hybrid polymer. This result clearly demonstrates the feasibility of this hybrid polymer participated homogeneous-to-heterogeneous phase change shape-stabilization strategy, which could not only be applied in organic PCMs but also feasible towards the synthesis of inorganic shape-stabilized PCMs.

Characterization regarding the synthesized shape-stabilized inorganic PCMs was then initiated. Similar with that of organic PCMs, FTIR and XRD patterns (**Fig. 5a** and **5b**) reveal that chemical structure of SAT was not damaged during this alkali induced hypercrosslinking reaction and the main response of the PCMs composite was attributed to the contribution of SAT inside. TGA patterns (**Fig. 5c**) were also in line with the mass fraction of the PCMs composite where the first weight loss was ascribed to the SAT inside and the second main weight loss was assigned to the hybrid polymer inside. It can be seen from **Fig. 5k** and **Fig. S7** that there are pores in the composite material and the mixture of sodium acetate trihydrate and carbon black is uniform.

This novel polymer supporting material prepared in the experiment has a stronger ability to cover inorganic material than organic material. In order to save material cost, we distinguish the molar ratio of organic composite material from that of organic composite material, and through experimental analysis, it is concluded that HP/CB-IPCMs (7:3) has a lower leakage rate and supercooling degree. It can be seen from **Fig. S8** and **Fig.5g** that after 15min, the leakage rate of HP/CB-IPCMs (7:3) was only 0.1%, and the supercooling degree was only 0.73°C. From the DSC data (**Fig. 5d** and **Fig. S6**), it can be seen that the enthalpy of all samples is relatively high, with the highest being 180.04 J/g. The pure SAT has two peaks in the melting process: solid-solid phase transition and solid-liquid phase transition. The overall enthalpy of phase transition is 224.73 J/g, and the temperature of phase transition is between 55-57°C. As shown in **Fig. 5g** and **5j**, it can be seen that the leakage rate of samples with different mole ratios decreased more than that of samples with different mass of hybrid polymer by changing the same law as that of organic composite materials. Therefore, we conclude that the hybrid polymer plays a very effective role in encapsulating organic or inorganic PCMs by changing the molar ratio of monomer. Supercooling degree is an important factor of inorganic PCMs application, we use the data collector in this topic, the pump and thermocouple sensor to test the inorganic composite materials in the process of solidification temperature change (**Fig. S11**). As can be seen from Table 5 and **Fig. 5e**, pure SAT the degree of supercooling about 15.98°C, and by adding hybrid polymer with carbon black after only 0.27°C of supercooling degree, it was basically eliminated the supercooling phenomenon of sodium acetate. Through research and analysis, the reason is that the three-dimensional network structure polymer formed through cross-linking not only serves as the supporting material of inorganic PCMs, but also provides more binding sites for inorganic PCMs in the solidification process, so that inorganic hydrated salt can solidify better.

Table 4 Data for the DSC curves for the HP/CB-IPCMs samples.

Sample	Onset(ºC)	Peak(ºC)
SAT	57.13	61.35
CB-IPCMs	56.22	59.60
HP/CB-IPCMs(9:1)	60.83	61.35
HP/CB-IPCMs(8.5:1.5)	55.41	61.54
HP/CB-IPCMs(8:2)	54.75	61.54
HP/CB-IPCMs(7.5:2.5)	57.30	61.30
HP/CB-IPCMs(7:3)	57.31	62.55

Table 5 Data for the supercooling degree curves for the HP/CB-IPCMs samples.

Sample	Freezing process		
	Theoretical phase change temperature(ºC)	Actual phase change temperature (ºC)	Supercooling degree(ºC)
SAT	55.24	39.26	15.98
CB-IPCMs	53.83	38.34	15.49
HP/CB-IPCMs(9:1)	55.61	48.98	6.63
HP/CB-IPCMs(8.5:1.5)	55.22	54.06	1.16
HP/CB-IPCMs(8:2)	54.53	54.21	0.32
HP/CB-IPCMs(7.5:2.5)	53.35	53.08	0.27
HP/CB-IPCMs(7:3)	53.89	53.17	0.73

The application of this strategy

In order to broaden the application range of the polymer prepared in this study in PCMs, we tested five kinds of thermal conductive nanoadditives (graphene, titanium dioxide, copper oxide, silicon carbide, and expanded graphite), which were commonly used in the study of shape-stabilized PCMs to demonstrate

the general adaptability of this strategy. The proportions of all materials are the same as the mass fractions of each material in HP/CB-OPCMs (5:5), which well illustrates the feasibility of our strategy. As it is seen from **Fig. 5h**, the leakage rate of the composite with graphene added is only 0.07% after three leakage tests because grapheme not only act as nanoadditives which can improve the thermal conductive, but can be considered as supporting material in order to encapsulate PCMs. As shown in the **Fig. 5i**, the thermal conductivity of PCM with graphene at room temperature is 1.21 W (m^{-1} K^{-1}), which is 6 times higher than that of pure paraffin. The thermal conductivity of the composite with expanded graphite can also reach 0.86 W (m^{-1} K^{-1}), but its leakage rate is relatively high. We analyzed the reasons why the addition of five different thermal conductivity nano-additives showed different leakage rates, On the one hand, the proportion of preparing PCMs composite is not suitable for all thermal conductivity nanoadditives, and on the other hand, other kinds of nanoadditives can not be used as supporting materials to encapsulate PCMs. For our strategy from homogeneous to heterogeneous, we only need a simple treatment to "lock" the PCMs, thus achieving the requirements of fixed shape PCMs. Initially, our strategy can be applied to different thermal conductivity nanoadditives, which can improve the thermal conductivity of composite materials.

In this paper, a kind of polymer containing organic/inorganic hybrid silioxyl functional group was successfully synthesized and applied to the encapsulation of PCMs. Due to the mildness of the hypercrosslinking reaction, only a small amount of aqueous alkali solution is required to be added to the tolerance of organic and inorganic PCMs. More importantly, the homogeneous start state of the mixture guarantees the highest encapsulation rate of the phase change material and the uniform blend of the nanoadditives. Further studies showed that the hybrid polymer gave the PCM a unique self-cleaning property, which made it a good hydrophobicity to water droplets. In addition, the PCMs encapsulation method is adapted to different nanoadditives, resulting in a 600% increase in maximum thermal conductivity and 93.7% increase in light-to-thermal conversion efficiency. The latent heat of 180 J/g of PCMs composite was observed without any leakage.

Methods

Materials. Paraffin wax (melting temperature is approximately 60 ºC) was purchased from Shanghai Joule Wax Co., LTD., China; Styrene (99%), 2, 2-azobis methylpropionitrile (AIBN, >98%) were purchased from Shanghai Adama Reagent Co., LTD., China. Trimethoxy(4-vinylphenyl)silane (97%) and dichloromethane (DCM, AR, 99.5%) were purchased from Shanghai Macklin Biochemical Technology Co., LTD in China. Carbon Black (MA100) was purchased from Mitsubishi Carbon Black of Japan with a 100m^2/g surface area of nitrogen attachment. Chloroform was purchased from National Medicines Corporation Ltd., China. Unless otherwise noted, all reagents were obtained from commercial suppliers and were used without further purification.

Hypercrosslinked polymer preparation process. The preparation was carried out in a 100ml beaker. Firstly, removing the stabilizer form PS by using Al_2O_3. Styrene (5g, 48mmol) was mixed with Trimethoxy(4-vinylphenyl)silane (TMVPS,1.2g,5.3mmol) and AIBN(15.8mg,0.96mmol) in chloroform (15ml). The

mixture was stirred for 12h at 80˚C with condensing and gas protection devices and then cooled to room temperature. The resulting polymer solution was slowly dripped into hexane, then the supernatant is removed after the crude copolymer precipitated, the resulted solid was dissolved in dichloromethane. The solution was dripped into hexane, and the same procedure repeated twice. After the aboving procedure, the purified copolymer was dried (12h at room temperature in *vacuo*) to obtain the final copolymer. The molar ration of the copolymer was determined by ^{1}H NMR spectroscopic analysis (x/y 9:1,8:2,7:3,6:4,5:5).

Preparation process of HP/CB-OPCMs composite. The reaction was carried out in a 250ml round-bottomed flask. Paraffin wax (5g) was put into the flask and allowed to heat to 80 ºC with condensing devices. Petroleum ether (10ml) was added into the flask after the paraffin wax was completely melting. Then carbon black (5g) was added into the flask at 80 ºC under magnetic stirring for 1h. The purified copolymer (0.5g) dissolved by Methylene chloride was slowly dripped into the flask and stirred for 20 min, then Saturated sodium hydroxide solution (1ml) was slowly dripped into the flask after the copolymer was completely dispersed. The reaction was finished when the mixture become solid. After the reaction, the solvent was evaporated off and the resulted composite HP/CB-OPCMs was obtained as a dark cake after drying in vacuum oven at 80 ºC for 12h.

Preparation process of HP/CB-IPCMs composite. The reaction was carried out in a 250ml round-bottomed flask. Sodium acetate trihydrate (20g) was put into the flask and allowed to heat to 70 ºC. Deionized water (0.5ml) was added into the flask after the sodium acetate trihydrate was completely melting. Then carbon balck (5g) was added into the flask at 70 ºC under magnetic stirring for 1h. The purified copolymer (0.5g) dissolved by Methylene chloride was slowly dripped into the flask and stirred for 20 min, then Saturated sodium hydroxide solution (1ml) was slowly dripped into the flask after the copolymer was completely dispersed. The reaction was finished when the mixture become solid. After the reaction, the solvent was evaporated off and the resulted composite HP/CB-IPCMs was obtained as a dark cake after drying at room temperature for 12h.

Characterization of materials. Fourier-transform infrared spectra (FT-IR) spectra were recorded as KBr discs by using a Bruker VERTEX 70 FT-IR spectrometer. Thermal gravimetric analysis (TGA) was carried out on a TA SDT Q600 instrument under a nitrogen atmosphere by heating from room temperature to 800 ºC at a rate of 10 ºC min^{-1}. Differential scanning calorimetry (DSC) was performed in a TA Q200 at a heating (or cooling) rate of 2 ºC min^{-1} under a nitrogen atmosphere. All the samples were heated to 70 ºC, then cooled to 10 ºC and equilibrated for 10 min. X-ray diffraction (XRD) patterns were recorded on a diffractometer (Smartlab, Rigaku) with Ni-filtered CuK α radiation (k = 0.154 nm) at a tube current of 30 mA and a generator voltage of 40 kV and performed at a speed of 8 ºC min^{-1}, from to 80 º of 2θ. Scanning electron microscopy (SEM) images were recorded using a FEI Sirion 200 field-emission scanning electron microscope operating at 10 kV. Thermal conductivity of the samples was measured by using a thermal conductivity meter (Hot Disk 2500-OT, Sweden), based on the transient plane source method, where the testing temperature was adjusted and controlled by a water bath and an insulated chamber. The surface areas were calculated from nitrogen adsorption data by Brunauer–Emmett–Teller (BET) or Langmuir analysis. Pore size distributions were calculated by density functional theoretical

(DFT) methods from the adsorption branch. Nuclear Magnetic Resonance Spectrometer (^{1}H NMR) was carried out on an AVANCE III HD 600 MHz instrument.

Declarations

Conflicts of interest

There are no conflicts to declare.

Acknowledgements

Thanks for financial support from the National Natural Science Foundation of China (No. 51906252) and the Natural Science Foundation of Jiangsu Province (NO. BK20190632), China Postdoctoral Science Foundation (2019M661980).

References

1. Wang CX, Hua LJ, Yan HZ, Li BJ, Tu YD, Wang RZ. A Thermal Management Strategy for Electronic Devices Based on Moisture Sorption-Desorption Processes. *Joule* **4**, 435-447 (2020).
2. Liu CH, Song Y, Xu Z, Zhao JT, Rao ZH. Highly efficient thermal energy storage enabled by a hierarchical structured hypercrosslinked polymer/expanded graphite composite. *Int J Heat Mass Transf* **148**, 11 (2020).
3. Liu CH*, et al.* A novel shape-stabilization strategy for phase change thermal energy storage. *J Mater Chem A* **7**, 8194-8203 (2019).
4. Liu CH*, et al.* Knitting aryl network polymers (KAPs)-embedded copper foam enables highly efficient thermal energy storage. *J Mater Chem A* **8**, 15177-15186 (2020).
5. Tan KW, Jung B, Werner JG, Rhoades ER, Thompson MO, Wiesner U. Transient laser heating induced hierarchical porous structures from block copolymer-directed self-assembly. *Science* **349**, 54-58 (2015).
6. Liu CH, Du PX, Fang B, Li ZY, Chen BH, Rao ZH. Experimental study on a functional microencapsulated phase change material for thermal management. *Int Commun Heat Mass* **118**, (2020).
7. Liu CH, Ma XT, Du PX, Rao ZH. Fabrication of highly efficient thermal energy storage composite from waste polystyrenes. *Chem Eng Sci* **216**, 11 (2020).
8. Liu CZ, Luo CY, Xu TT, Lv PZ, Rao ZH. Experimental study on the thermal performance of capric acid-myristyl alcohol/expanded perlite composite phase change materials for thermal energy storage *Sol Energy* **191**, 585-595 (2019).
9. Liu CZ, Rao ZH. Challenges in various thermal energy storage technologies. *Sci Bull* **62**, 231-233 (2017).

10. Zhang YF*, et al.* Broadband transparent optical phase change materials for high-performance nonvolatile photonics. *Nat Commun* **10**, 9 (2019).
11. Zhou D, Zhao CY, Tian Y. Review on thermal energy storage with phase change materials (PCMs) in building applications. *Appl Energy* **92**, 593-605 (2012).
12. Zhou L, Tang LS, Tao XF, Yang J, Yang MB, Yang W. Facile fabrication of shape-stabilized polyethylene glycol/cellulose nanocrystal phase change materials based on thiol-ene click chemistry and solvent exchange. *Chem Eng J* **396**, 10 (2020).
13. Zhang P, Xiao X, Ma ZW. A review of the composite phase change materials: Fabrication, characterization, mathematical modeling and application to performance enhancement. *Appl Energy* **165**, 472-510 (2016).
14. Zhang R*, et al.* Preparation of PEGA grafted poly(chloromethylstyrene-co-ethylene glycol dimethacrylate) monolith for high-efficiency solid phase peptide synthesis under continuous flow techniques. *Polymer* **61**, 115-122 (2015).
15. Zhang Y*, et al.* Ag-graphene/PEG composite phase change materials for enhancing solar-thermal energy conversion and storage capacity. *Appl Energy* **237**, 83-90 (2019).
16. Babaei H*, et al.* Observation of reduced thermal conductivity in a metal-organic framework due to the presence of adsorbates. *Nat Commun* **11**, (2020).
17. Feng L*, et al.* n-Dodecanol nanocapsules with supramolecular lock shell layer for thermal energy storage. *Chem Eng J* **389**, 12 (2020).
18. Gao HY*, et al.* Nanoconfinement effects on thermal properties of nanoporous shape-stabilized composite PCMs: A review. *Nano Energy* **53**, 769-797 (2018).
19. Huang H, Shi T, He R, Wang J, Chu PK, Yu X-F. Phase-Changing Microcapsules Incorporated with Black Phosphorus for Efficient Solar Energy Storage. *Adv Sci* **7**, (2020).
20. Huang WC*, et al.* Efficient and Mechanically Robust Ultraflexible Organic Solar Cells Based on Mixed Acceptors. *Joule* **4**, 128-141 (2020).
21. Huo YT, Guo YQ, Rao ZH. Investigation on the thermal performance of phase change material/porous medium-based battery thermal management in pore scale. *Int J Energy Res* **43**, 767-778 (2019).
22. Kim H*, et al.* Water harvesting from air with metal-organic frameworks powered by natural sunlight. *Science* **356**, 430-432 (2017).
23. Kim S, Drza LT. High latent heat storage and high thermal conductive phase change materials using exfoliated graphite nanoplatelets. *Sol Energy Mater Sol Cells* **93**, 136-142 (2009).
24. Koo D*, et al.* Flexible Organic Solar Cells Over 15% Efficiency with Polyimide-Integrated Graphene Electrodes. *Joule* **4**, 1021-1034 (2020).
25. Du XS, Qiu JH, Deng S, Du ZL, Cheng X, Wang HB. Flame-retardant and form-stable phase change composites based on black phosphorus nanosheets/cellulose nanofiber aerogels with extremely

high energy storage density and superior solar-thermal conversion efficiency. *J Mater Chem A* **8**, 14126-14134 (2020).

26. Du XS, Qiu JH, Deng S, Du ZL, Cheng X, Wang HB. Alkylated Nanofibrillated Cellulose/Carbon Nanotubes Aerogels Supported Form-Stable Phase Change Composites with Improved n-Alkanes Loading Capacity and Thermal Conductivity. *ACS Appl Mater Interfaces* **12**, 5695-5703 (2020).
27. Kawaguchi T, Sakai H, Sheng N, Kurniawan A, Nomura T. Microencapsulation of Zn-Al alloy as a new phase change material for middle-high-temperature thermal energy storage applications. *Appl Energy* **276**, (2020).
28. Liu MK*, et al.* Conductive carbon nanofiber interpenetrated graphene architecture for ultra-stable sodium ion battery. *Nat Commun* **10**, 11 (2019).
29. Liu YD, Zhou YG, Tong MW, Zhou XS. Experimental study of thermal conductivity and phase change performance of nanofluids PCMs. *Microfluid Nanofluidics* **7**, 579-584 (2009).
30. Luo B, Ye DL, Wang LZ. Recent Progress on Integrated Energy Conversion and Storage Systems. *Adv Sci* **4**, 15 (2017).
31. Wei YH, Li JJ, Sun FR, Wu JR, Zhao LJ. Leakage-proof phase change composites supported by biomass carbon aerogels from succulents. *Green Chem* **20**, 1858-1865 (2018).
32. Wu S*, et al.* Highly thermally conductive and flexible phase change composites enabled by polymer/graphite nanoplatelet-based dual networks for efficient thermal management. *J Mater Chem A* **8**, 20011-20020 (2020).
33. Wu S*, et al.* High-Performance Thermally Conductive Phase Change Composites by Large-Size Oriented Graphite Sheets for Scalable Thermal Energy Harvesting. *Adv Mater* **31**, 9 (2019).
34. Fang H*, et al.* Fibrous form-stable phase change materials with high thermal conductivity fabricated by interfacial polyelectrolyte complex spinning. *Carbohydr Polym* **249**, (2020).
35. Tauseef ur R, Ali HM, Janjua MM, Sajjad U, Yan WM. A critical review on heat transfer augmentation of phase change materials embedded with porous materials/foams. *Int J Heat Mass Trans* **135**, 649-673 (2019).
36. Wang SL*, et al.* Porous hypercrosslinked polymer-TiO2-graphene composite photocatalysts for visible-light-driven CO2 conversion. *Nat Commun* **10**, 10 (2019).
37. Fallahi A, Guldentops G, Tao MJ, Granados-Focil S, Van Dessel S. Review on solid-solid phase change materials for thermal energy storage: Molecular structure and thermal properties. *Appl Therm Eng* **127**, 1427-1441 (2017).
38. Min P*, et al.* Thermally Conductive Phase Change Composites Featuring Anisotropic Graphene Aerogels for Real-Time and Fast-Charging Solar-Thermal Energy Conversion. *Adv Funct Mater* **28**, 9 (2018).
39. Zan GT, Wu QS. Biomimetic and Bioinspired Synthesis of Nanomaterials/Nanostructures. *Adv Mater* **28**, 2099-2147 (2016).

40. Mohamed SA*, et al.* A review on current status and challenges of inorganic phase change materials for thermal energy storage systems. *Renew Sust Energ Rev* **70**, 1072-1089 (2017).
41. Zhang N, Yuan YP, Cao XL, Du YX, Zhang ZL, Gui YW. Latent Heat Thermal Energy Storage Systems with Solid-Liquid Phase Change Materials: A Review. *Adv Eng Mater* **20**, 30 (2018).
42. Prieto I*, et al.* High quality factor GaAs-based photonic crystal microcavities by epitaxial re-growth. *Opt Express* **21**, 31615-31622 (2013)
43. Shukla A, Buddhi D, Sawhney RL. Thermal cycling test of few selected inorganic and organic phase change materials. *Renew Energ* **33**, 2606-2614 (2008).
44. Zhang M*, et al.* Plasmonic Metasurfaces for Switchable Photonic Spin-Orbit Interactions Based on Phase Change Materials. *Adv Sci* **5**, 8 (2018).
45. Reb LK*, et al.* Perovskite and Organic Solar Cells on a Rocket Flight. *Joule* **4**, 1880-1892 (2020).
46. Rutz AL, Hyland KE, Jakus AE, Burghardt WR, Shah RN. A Multimaterial Bioink Method for 3D Printing Tunable, Cell-Compatible Hydrogels. *Adv Mater* **27**, 1607-1614 (2015).
47. Soares N, Costa JJ, Gaspar AR, Santos P. Review of passive PCM latent heat thermal energy storage systems towards buildings' energy efficiency. *Energy Build* **59**, 82-103 (2013).
48. Qiu JC, Huo D, Xia YN. Phase-Change Materials for Controlled Release and Related Applications. *Adv Mater* **32**, 21 (2020).
49. Du XS, Xu JI, Deng S, Du ZL, Cheng X, Wang HB. Amino-Functionalized Single-Walled Carbon Nanotubes-Integrated Polyurethane Phase Change Composites with Superior Photothermal Conversion Efficiency and Thermal Conductivity. *ACS Sustain Chem Eng* **7**, 17682-17690 (2019).
50. Du XS, Zhou M, Deng S, Du ZL, Cheng X, Wang HB. Poly(ethylene glycol)-grafted nanofibrillated cellulose/graphene hybrid aerogels supported phase change composites with superior energy storage capacity and solar-thermal conversion efficiency. *Cellulose* **27**, 4679-4690 (2020).
51. Mishra AK, Lahiri BB, Philip J. Carbon black nano particle loaded lauric acid-based form-stable phase change material with enhanced thermal conductivity and photo-thermal conversion for thermal energy storage. *Energy* **191**, 15 (2020).
52. Yang J, Jia YL, Bing NC, Wang LL, Xie HQ, Yu W. Reduced graphene oxide and zirconium carbide co-modified melamine sponge/paraffin wax composites as new form-stable phase change materials for photothermal energy conversion and storage. *Appl Therm Eng* **163**, 9 (2019).
53. Yang L, Yuan YP, Zhang N, Dong YF, Sun YF, Ji WH. Photo-to-thermal conversion and energy storage of lauric acid/expanded graphite composite phase change materials. *Int J Energy Res* **44**, 8555-8566 (2020).
54. Fan ZM*, et al.* Modified MXene/Holey Graphene Films for Advanced Supercapacitor Electrodes with Superior Energy Storage. *Adv Sci* **5**, 11 (2018).
55. Fang M, Chen GM. Effects of different multiple PCMs on the performance of a latent thermal energy storage system. *Appl Therm Eng* **27**, 994-1000 (2007).

56. Lin YX, Jia YT, Alva G, Fang GY. Review on thermal conductivity enhancement, thermal properties and applications of phase change materials in thermal energy storage. *Renew Sust Energ Rev* **82**, 2730-2742 (2018).
57. Mo Z*, et al.* Ti(3)C(2)Tx@Polyvinyl alcohol foam-Supported Phase Change Materials with Simultaneous Enhanced Thermal Conductivity and Solar-Thermal Conversion Performance. *Sol Energy Mater Sol Cells* **219**, (2021).
58. Sheng N*, et al.* Anisotropically enhanced heat transfer properties of phase change material reinforced by graphene-wrapped carbon fibers. *Sol Energy Mater Sol Cells* **206**, 9 (2020).
59. Yuan KJ*, et al.* Engineering the Thermal Conductivity of Functional Phase-Change Materials for Heat Energy Conversion, Storage, and Utilization. *Adv Funct Mater* **30**, 31 (2020).
60. Yang JM, Kim JS. The microencapsulation of calcium chloride hexahydrate as a phase-change material by using the hybrid coupler of organoalkoxysilanes. *J Appl Polym Sci* **135**, 10 (2018).
61. Fu WW*, et al.* Preparation and properties of phase change temperature-tuned composite phase change material based on sodium acetate trihydrate-urea/fumed silica for radiant floor heating system. *Appl Therm Eng* **162**, 10 (2019).
62. Xiao QQ, Fan JX, Li L, Xu T, Yuan WH. Solar thermal energy storage based on sodium acetate trihydrate phase change hydrogels with excellent light-to-thermal conversion performance. *Energy* **165**, 1240-1247 (2018).

Figures

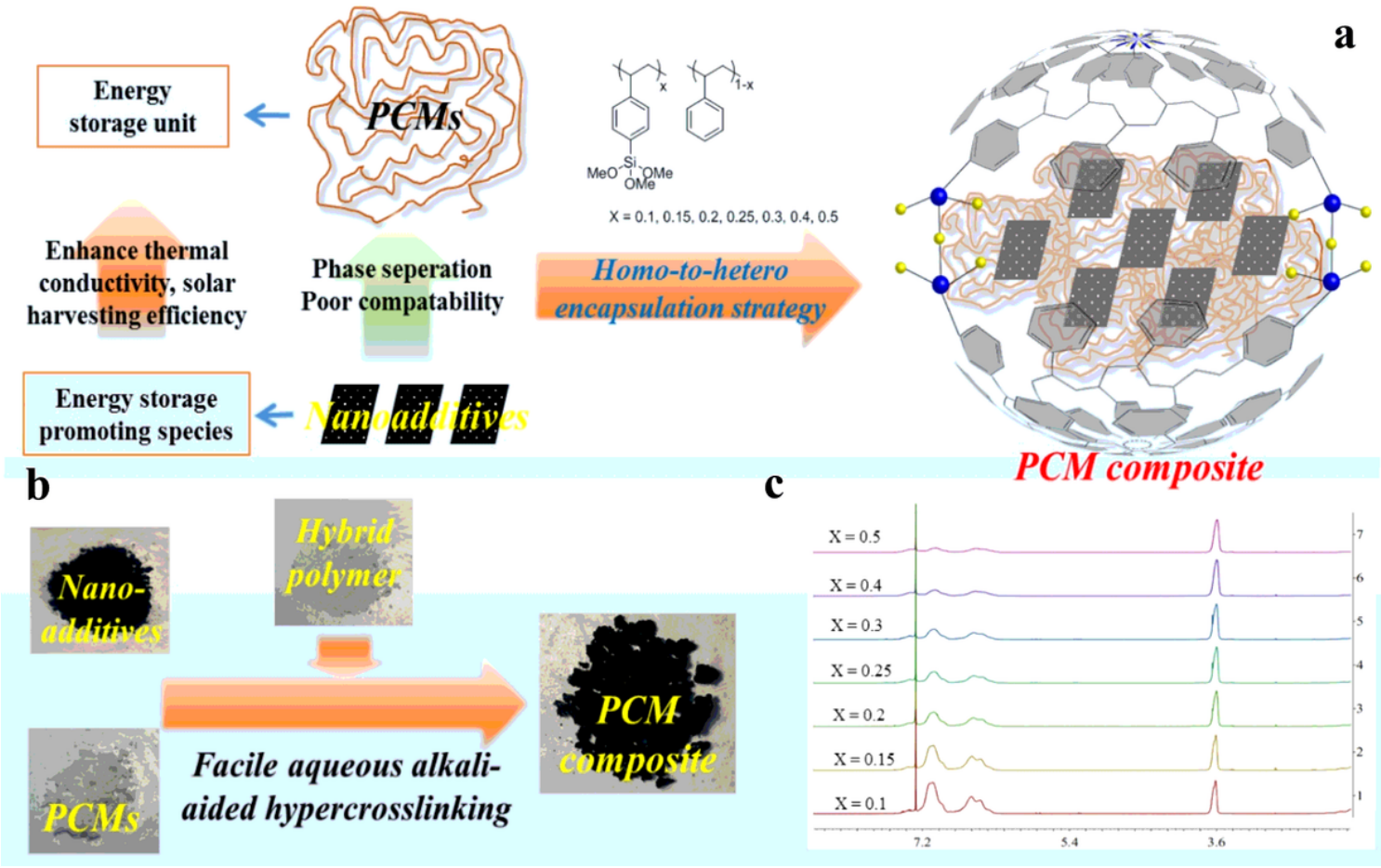

Figure 1

Schematic illustration of the preparation procedure of HP/CB-OPCMs composite; (a) The synthetic concept of HP/CB-PCMs; (b) Facile aqueous alkali aided hypercrosslinking hybrid polymer PCMs encapsulation; (c) 1H NMR spectra of different hybrid polymers.

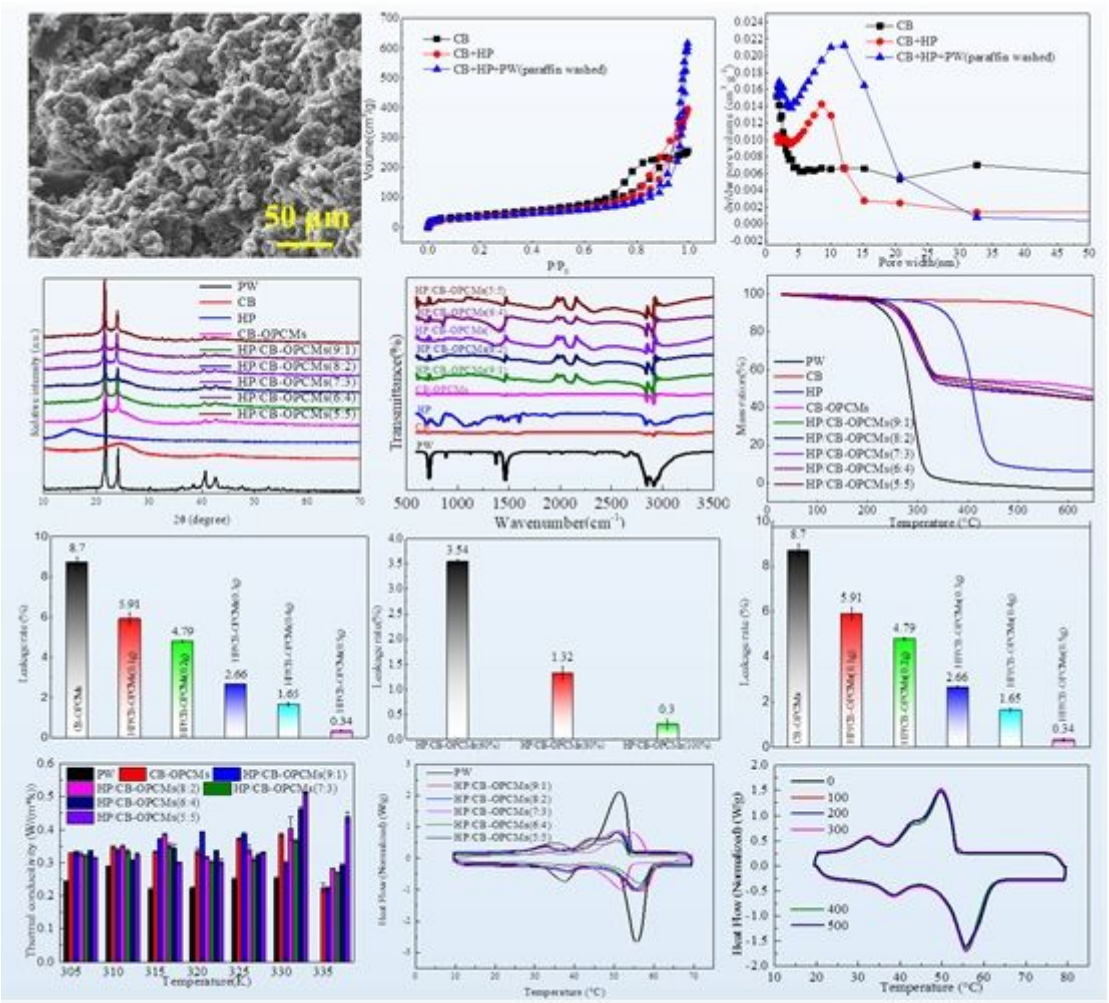

Figure 2

Structure and porosity of HP/CB-OPCMs (a) SEM images of HP/CB-OPCMs; (b) nitrogen adsorption and desorption isotherms at 77.3 K of HP/CB-OPCMs; (c) pore size distribution of HP/CB-OPCMs; (d) XRD images of HP/CB-OPCMs; (e) FT-IR images of HP/CB-OPCMs; (f) TGA images of HP/CB-OPCMs; (g) Leakage rates of PCMs composite with different proportions of polymer monomers; (h) Leakage rates of PCMs composite with different proportions of supporting materials; (i) Leakage rates of PCMs composite with different polymer masse; (j) the thermal conductivity of the HP/CB-OPCMs samples; (k) DSC curves of the melting and freezing process of pure paraffin and HP/CB-OPCMs; (l) the measured latent heat of HP/CB-OPCMs(5:5) during 500 melting-freezing cycles.

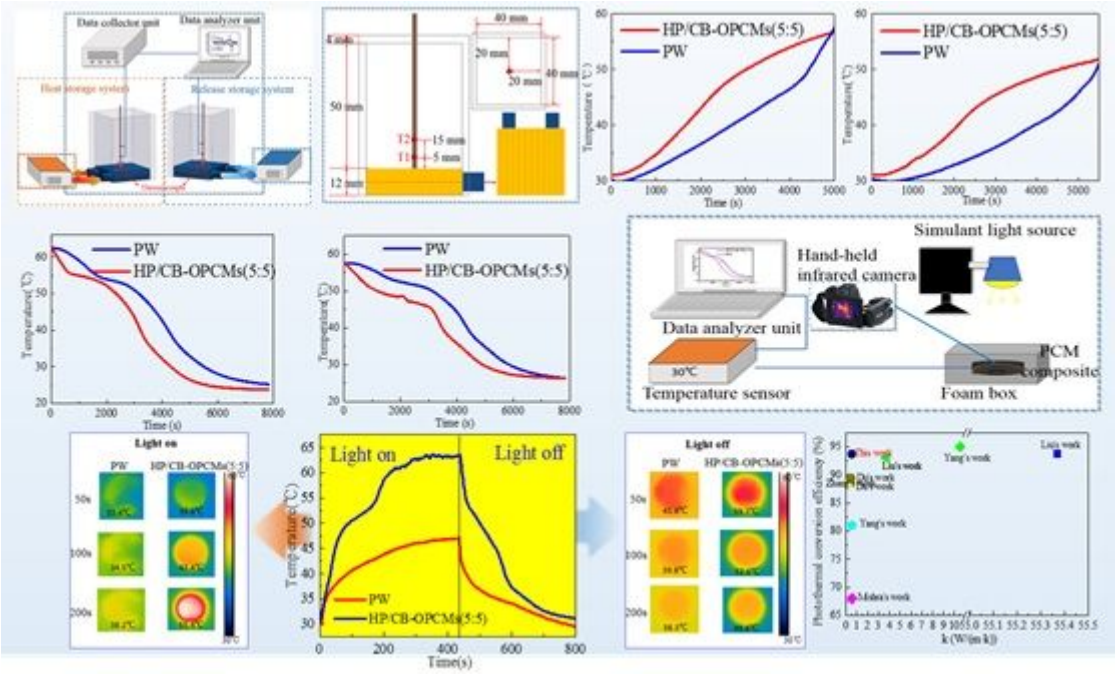

Figure 3

Energy storage and release performance comparison between paraffin and HP/CB-OPCMs(5:5). (a) Schematic diagram of the thermal energy storage and release tests; (b) the site and detail size of the thermocouples and heat storage chamber, and the thermal storage properties of HP/CB-OPCMs(5:5) at site 1 (c) and site 2 (d) and the thermal storage properties of HP/CB-OPCMs(5:5) at site 1 (e) and site2 (f); (g) Schematic illustration of the light-to-thermal energy conversion and storage measuring platform; (i) Light-to-thermal energy conversion curves for pure paraffin and HP/CB-OPCMs(5:5); Heat transfer rate of paraffin and HP/CB-OPCMs(5:5) during (h) light-on and (J) light-off process; (K) Comparison of research work between different scholars.2, 4, 15, 49, 50, 51, 52, 53

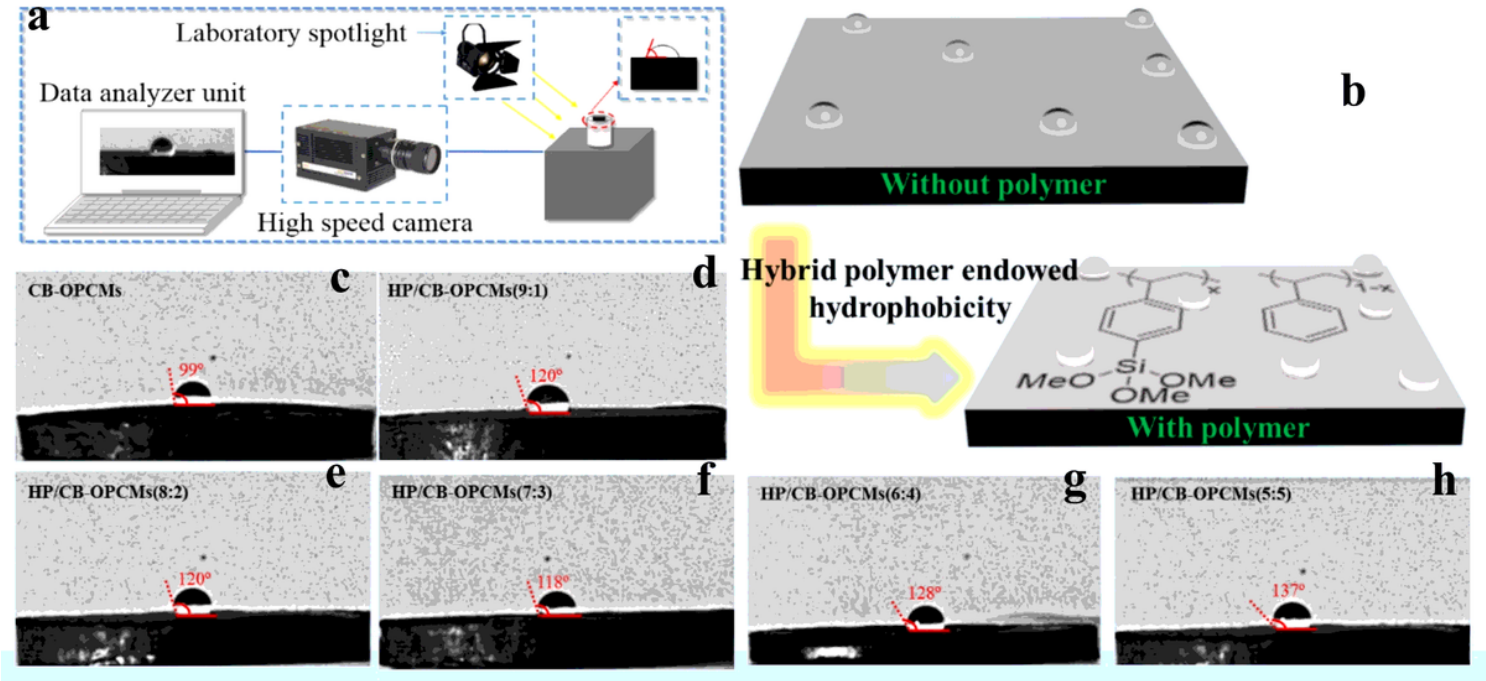

Figure 4

(a) Schematic illustration of the contact Angle platform. (b) Experimental diagram of contact Angle of CB-OPCMs; (c) CB-PCMs; (d) HP/CB-OPCMs(9:1); (e) HP/CB-OPCMs(8:2); (f) HP/CB-OPCMs(7:3); (g) HP/CB-OPCMs(6:4); (h) HP/CB-OPCMs(5:5).

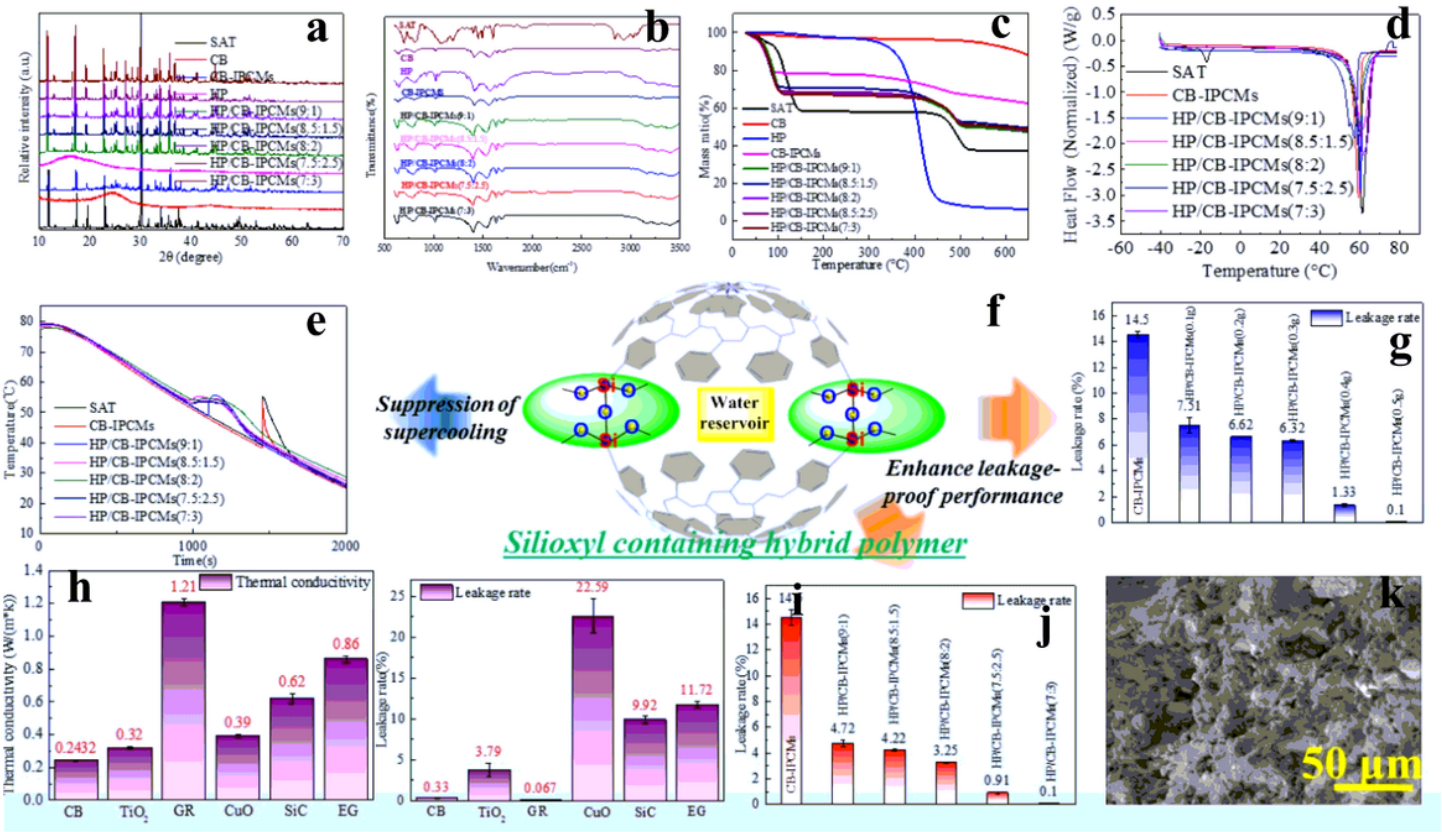

Figure 5

Chemical structure and thermophysical performance of HP/CB-IPCMs. (a) XRD images of HP/CB-IPCMs; (b) FTIR images of HP/CB-IPCMs; (c) TGA images of HP/CB-IPCMs; (d) DSC curves of the melting and freezing process of pure SAT and HP/CB-IPCMs; (e) The supercooling degree of HP/CB-IPCMs; (f) Schematic diagram of water storage with hybrid polymer; (g) Leakage rates of HP/CB-IPCMs with different proportions of polymer monomers; (h) Data graph of leakage rate of polymer composites with different nanoadditives; (i) Data graph of thermal conductivity of polymer composites with different nanoadditives; (j) Leakage rates of HP/CB-IPCMs with different polymer masse; (k) SEM images of HP/CB-IPCMs.

Supplementary Files

This is a list of supplementary files associated with this preprint. Click to download.

- leakagevideo.mp4

- Supportingmaterials20210112.XXX.docx